CHAPTER 5

Mass Balance Processes: 2. Surface Ablation and Energy Budget

> "It was as hot a day as we had ever had. The temperature was 36° Fahr. in the shade. . . . This had an awful effect on the surface, covering it with pools and making it very treacherous to walk upon"
>
> ***South: The Endurance Expedition*, Ernest Shackleton**

5.1 Introduction

In the complex relationship between glaciers and climate, one of the key processees is melt of snow and ice at the glacier surface. Melting followed by runoff accounts for most of the ablation on many glaciers. The runoff itself is an important water resource downstream, for agriculture, domestic uses, and power generation.

The total melt over the course of a year generally increases in warmer climates. In particular melt increases with summer temperatures. For this reason, the surface mass balance turns strongly negative when glaciers flow to low altitudes (as seen in Figure 4.6) or when ice sheets expand toward low latitudes. And increased melt drives glacier retreat when climate warms. But temperatures alone do not determine melt. Wind speed, humidity, clouds, snowfalls, surface characteristics, and other variables all play a role. Moreover, their effects are partly interdependent. As one consequence, all of these variables not only influence melt directly but also influence the sensitivity of melt to warming.

In the previous chapter we reviewed all the factors that determine glacier mass balance, but neglected the details of melt and its relation to climate – the subject of the present chapter. In very cold environments, sublimation replaces melt as the primary mechanism of surface ablation. We discuss sublimation here as well. To understand the causes of ablation by melting and sublimation, we need to examine the ways in which the glacier surface gains and loses heat and be able to measure or calculate the gains and losses under different weather conditions. The theoretical treatment of heat exchange at the surface makes drastic simplifying assumptions about how to represent rapidly fluctuating processes involving many variables. For the long-timescale problems most relevant to glacier evolution, the use of simple empirical relations is a valuable alternative. Here we outline the full theory and discuss the factors controlling

DOI: 10.1016/B978-0-12-369461-4.00005-3

each term in the energy budget, using field examples. We then discuss the relation between surface ablation and climate: the simplified approaches used in glacier models, the importance of variable weather conditions, and the contrasts between energy budgets of glaciers in different regions. We begin by reviewing a few fundamental concepts.

5.1.1 Radiation

All matter radiates electromagnetic energy to its surroundings. A material that emits the maximum possible amount of radiation for its temperature is known as a *perfect radiator*. Because such a material also absorbs all the radiation that falls on it, a perfect radiator is also known as a *black body*, and the radiation from it is referred to as black-body radiation. Snow behaves as a nearly perfect radiator in the infrared part of the spectrum. The intensity of the radiation emitted by a perfect radiator depends only on its temperature. The Stefan-Boltzman Law gives the radiated energy flux E (energy per unit area per unit time, $\mathrm{W\,m^{-2}}$) as

$$E = \sigma T^4, \tag{5.1}$$

for absolute temperature T. *Stefan's constant*, the parameter σ, has a value of $5.67 \times 10^{-8}\,\mathrm{W\,m^{-2}\,K^{-4}}$. The radiation is distributed over a band of wavelengths. The wavelength of maximum flux λ_m, the peak of the spectrum, is inversely proportional to T. For nonperfect radiators, a factor ϵ, the *emissivity*, appears as an additional coefficient multiplying the right-hand side of Eq. 5.1. The emissivity is the ratio of the actual flux to that emitted by a perfect radiator at the same temperature. Although snow reflects visible light abundantly, it nonetheless has an emissivity close to one because it emits mostly at infrared wavelengths.

To a good approximation, the sun and the Earth's surface behave as perfect radiators. The sun has an effective temperature of about 6000 K and λ_m of about 0.5 μm; this lies in the visible part of the spectrum. The Earth's effective temperature is slightly less than 300 K and λ_m falls in the infrared spectrum at about 10 μm. The spectra of solar and terrestrial radiation overlap very little; 99% of solar energy lies between wavelengths of 0.15 and 4 μm, largely in the visible range, whereas 99% of terrestrial radiation is infrared, between 4 and 120 μm. The two bands are referred to as *shortwave* and *longwave* radiation. The instruments used in field studies to measure radiation, known as *radiometers*, give values integrated over a band of wavelengths, typically 0.3 to 2.8 μm for shortwave and 5 to 50 μm for longwave.

5.1.2 Energy Budget of Earth's Atmosphere and Surface

The sun is the ultimate source of almost all heat received at the Earth's surface (geothermal sources being negligible, except locally). The flux of energy toward Earth – above the atmosphere and at normal incidence – defines the *solar constant*, with a value of approximately $1367\,\mathrm{W\,m^{-2}}$. The Earth's surface usually receives less than this, even when the sun is directly overhead, because some radiation scatters back to space and some is absorbed by clouds, water vapor,

particles, and ozone in the atmosphere. In addition, some of the radiation reaching the surface reflects back; how much depends on the nature of the surface. At the same time, the Earth's surface emits longwave radiation. Some of it escapes to space and the atmosphere absorbs the remainder, mainly in clouds, water vapor, and carbon dioxide. These clouds and gases also emit longwave radiation. Although some escapes to space and some is reabsorbed in the atmosphere, a substantial amount of reradiated longwave energy returns to the Earth's surface (the *greenhouse effect*). Because the Earth acts as a perfect radiator in the infrared, nearly all of this returned radiation is absorbed at the surface and so contributes to warming or melting of ice. The natural greenhouse effect increases the Earth's surface temperature by about 30 °C; it is a major factor in the climate.

Several additional processes transfer heat between the Earth's surface and atmosphere. Turbulent eddies bring heat to the surface if the air is warmer than the surface or remove heat if the air is colder (processes known as *sensible heat transfer*). In addition, the surface receives latent heat when atmospheric water vapor condenses on it and loses heat when moisture evaporates or sublimates from it. The amount of heat transferred by these processes increases with the vigor of turbulence in the air flowing along the surface. Underground conduction also transfers sensible heat to or from the surface, and precipitation brings additional sensible heat.

Figure 5.1 diagrams the flow of energy through the atmosphere and its exchanges with the surface; values are averaged for the planet and an annual cycle. The left-hand side of the diagram shows shortwave radiation, the right-hand side shows longwave. The longwave "back radiation" is the greenhouse effect. At some times and places, the longwave back-radiation exceeds the surface radiation, giving a net longwave flux toward the surface – opposite from the diagram. Likewise, at some times and places the fluxes of sensible heat ("thermals") and latent heat ("evapotranspiration") are directed toward the surface rather than away from it. Note the size of the greenhouse effect; on average only a fraction 4/35 (about 11%) of the longwave radiation from the surface escapes directly to space. Note too that where the surface is snow or ice, it reflects a larger fraction of total incoming solar radiation than the 9% average shown.

At the surface, the absorbed solar radiation approximately balances the upward fluxes of longwave radiation and sensible and latent heat. An exact balance, however, would occur only if the radiation, the weather, and the surface conditions did not change. Usually, in fact, the surface gains or loses energy – the surface receives a *net energy flux* that warms or cools the ground, melts snow and ice, or causes freezing. Particularly large net energy fluxes occur with the daily and seasonal cycles of atmospheric conditions.

If the surface is snow or ice, and its temperature at melting point, a positive net energy flux produces further melt. Melt on glaciers is thus favored by the following factors, in particular:

1. Strong sunlight – as at mid-day under clear skies – increases absorbed solar radiation.
2. Low reflectivity – for example, where the surface is wet ice rather than dry snow – also increases absorbed solar radiation.

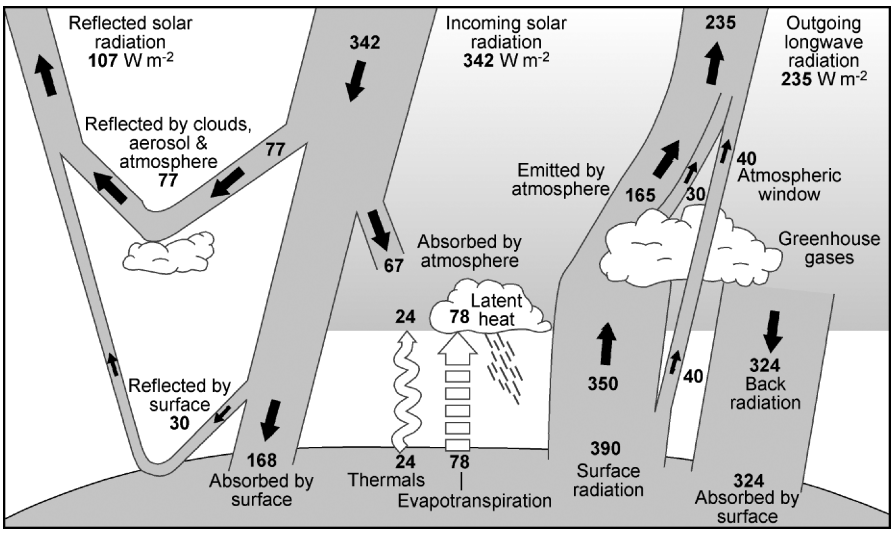

Figure 5.1: The energy flow through Earth's atmosphere and exchange with the surface – averaged for the globe and a year. All units are W m^{-2}. The numbers are constrained by satellite observations at the top of the atmosphere. Partitioning within the atmosphere is estimated from radiation models. Redrawn from Kiehl and Trenberth (1997). © American Meteorological Society.

3. A warm atmosphere – as during warm summer weather – increases both the greenhouse radiation and the sensible heat transfer to the surface.

4. A moist atmosphere increases greenhouse radiation and reduces latent heat losses from the surface. (On the other hand, increased moisture might enhance cloud cover and block sunlight.)

Persistence of all these factors favors melt ablation, the integral of melt rate over time.

5.2 Statement of the Surface Energy Budget

Define energy fluxes as positive when they represent a flow of energy to the snow/firn/ice surface. We are concerned with fluxes to and from a unit area of the surface – properly, each flux is a "flux density" – so units are energy per unit time per unit area, or W m^{-2}. Assuming no horizontal transfers of heat on the ground, the net energy flux into the surface, E_N, sums the following components:

$$E_N = \underbrace{E_S^{\downarrow} + E_S^{\uparrow} + E_L^{\downarrow} + E_L^{\uparrow}}_{E_{\mathbf{R}}} + E_G + E_H + E_E + E_P. \tag{5.2}$$

Here $E_S^{\downarrow}$ denotes the downward shortwave radiation, $E_S^{\uparrow}$ the reflected shortwave radiation, and $E_L^{\downarrow}$ and $E_L^{\uparrow}$ the downward and emitted longwave radiations; the sum of all the radiations

gives the *net radiation*, $E_{\mathbf{R}}$. E_G is the subsurface energy flux. E_H and E_E represent the sensible and latent heat fluxes due to turbulent mixing of the air adjacent to the surface. E_P represents the heat flux from precipitation, especially that which freezes. E_P is usually small and we will not discuss it further.[1]

In glacier studies, by convention, the latent heat flux E_E refers only to latent heat associated with vapor: that is, the heat consumed by evaporation and sublimation and released by condensation and deposition. The latent heat associated with melt and refreeze is part of E_N.

Equation 5.2 is usually referred to as the energy budget for "the surface," but practically it must apply to a layer of snow or ice with a finite thickness Δz. The term E_G measures the net energy flux through the bottom of this layer (by conduction and radiation) and its value depends on the choice of Δz. By choosing a Δz large enough so that seasonal temperature variations do not reach the bottom of the layer, we can approximate $E_G \approx 0$. Note that Eq. 5.2 does not include any terms for the energy content of meltwater flowing out of the layer; E_N already includes the energy for production of melt.

5.2.1 Driving and Responding Factors in the Energy Budget

The complexity of factors contributing to the energy budget sometimes threatens to obscure the underlying simplicity of the problem. The following summary – although not always strictly true – can be kept in mind.

Two factors primarily contribute energy to a melting glacier: sunlight and the atmosphere's heat content. The former corresponds to the downward shortwave radiation, the latter determines both the downward longwave radiation and the sensible heat transfer. Because of these energy flows to the glacier, its surface is kept "warm" – at a temperature roughly comparable to the overlying atmosphere. At the same time, the glacier continuously returns energy to its surroundings; the glacier would cool catastrophically if the inflows of energy were shut off. The biggest losses depend on the properties of the surface itself. The temperature determines the emitted longwave radiation, and the reflectivity determines the upward shortwave radiation. The atmosphere also robs some heat from the glacier by evaporation and sublimation into dry air and, at times, by sensible heat transfer into cold air. Finally, the temperature of the surface continuously tries to equilibrate with the temperature of the underlying ice, so some heat flows by conduction to or from the surface.

5.2.2 Melt and Warming Driven by Net Energy Flux

If the surface has warmed to the melting point, a positive E_N drives melt and a negative E_N drives freezing (if water is available). The total melt rate for the layer, $\dot{m}_s$, given as water-equivalent

[1] In temperate climates, devastating winter floods sometimes occur when rain falls on snow. It is a common misconception that such floods result from melt of snow by the rain. In fact, the principal reason for the floods is water saturation of the snowpack; rain quickly flows into the river channels because it cannot infiltrate the saturated snow and underlying soil. This is a type of *saturation overland flow*.

Table 5.1: Some thermodynamic parameters relevant to the surface energy budget.

Parameter	Symbol	Value	Units
Pure Ice (0 °C)			
density	ρ_i	917	$\mathrm{kg\,m^{-3}}$
specific heat capacity	c_i	2050	$\mathrm{J\,kg^{-1}\,K^{-1}}$
latent heat of fusion	L_f	3.34×10^5	$\mathrm{J\,kg^{-1}}$
latent heat of sublimation	L_s	28.3×10^5	$\mathrm{J\,kg^{-1}}$
Water (0 °C)			
density	ρ_w	1000	$\mathrm{kg\,m^{-3}}$
specific heat capacity	c_w	4218	$\mathrm{J\,kg^{-1}\,K^{-1}}$
latent heat of evaporation	L_v	2.5×10^6	$\mathrm{J\,kg^{-1}}$

thickness per unit time, is related to E_N by

$$\rho_w L_f \dot{m}_s \,[1 - f_r] + \int_0^{\Delta z} \rho c \frac{\partial T}{\partial t}\, dz = E_N. \tag{5.3}$$

$\dot{m}_s$ is positive for melt, negative for freezing. In the first term, ρ_w is the density of water, and L_f the latent heat of fusion for ice. The parameter f_r indicates the fraction of melt that refreezes within the layer; it ranges from zero to one. The second term represents the rate of gain of sensible heat in a vertical column of unit area through the layer, with ρ the density, c the specific heat capacity, T the temperature, and t time. Values for some of the thermodynamic parameters are listed in Table 5.1. (See Chapter 2 for a discussion of densities in general.)

If temperatures have reached the melting point throughout the layer, then the second term equals zero, f_r equals zero, and the ablation rate is simply $\dot{m}_s = E_N/\rho_w L_f$: such conditions often occur in summer in the ablation zones of temperate glaciers. If the entire layer is colder than melting point, the first term equals zero and the layer's temperature changes in proportion to E_N. If the surface is at melting point, but the layer underneath subfreezing, melt produced at the surface can percolate downward and partly refreeze, forming ice layers. This process releases latent heat and warms the layer. The larger the fraction that refreezes (f_r), the more the net energy goes to warming the layer. The net ablation rate $\dot{m}_s\,[1 - f_r]$ and gross melt $\dot{m}_s$ are in this case given by all the terms in Eq. 5.3. The warming due to refreezing can significantly affect temperatures in the firn (Section 9.3).

5.3 Components of the Net Energy Flux

In this section we discuss the separate terms in the surface energy budget, with an emphasis on conditions in a summer melt season.

Cold winter snowpacks delay the start of the melt season, as snow must first warm to its melting point before melting occurs. This process introduces a delay to the onset of melt.

Consider a 1-m-deep snowpack with a mean temperature of $-20\,°C$, a density of $500\,kg\,m^{-3}$, and a heat capacity of $2000\,J\,kg^{-1}\,K^{-1}$. With a net energy flux of $E_N = 50\,W\,m^{-2}$, it takes about 110 hours to warm the snowpack to melting point. This same amount of energy would melt about 0.06 m (w.eq.), much smaller than the few meters per year typical for glacier ablation zones. The transient warming of the winter snowpack is therefore a small factor in the annual energy budget, except in very cold regions.

Once the snow or ice surface starts to melt, the loss of energy by emitted longwave radiation $E_L^{\uparrow}$ cannot increase further because the surface temperature cannot rise above the melting point. Three factors then drive melt: increases of net shortwave radiation ($E_S^{\text{Net}} = E_S^{\downarrow} - E_S^{\uparrow}$), increases of downward longwave radiation, and increases of sensible heat transfer. The latter two processes increase, in turn, with temperature of the overlying atmosphere. When melt removes snow to expose ice, the surface absorbs more shortwave radiation, increasing E_S^{Net}. For these reasons, all three energy sources contribute to increasing ablation when the summertime climate warms (Section 5.4). But ablation might also increase because of other factors, such as reduced mid-day cloud cover.

5.3.1 Downward Shortwave Radiation

The flux of solar energy toward Earth at the top of the atmosphere approximately equals the solar constant; it varies by a few percent over a year because of the eccentricity of Earth's elliptical orbit. As it traverses the atmosphere, solar radiation is partly scattered and absorbed by gases, water droplets, ice crystals, and particles. The total solar flux reaching the ground ($E_S^{\downarrow}$), often called the *insolation* or the *global radiation*, adds together three components: the direct solar beam, the diffuse light arriving from all directions in the sky due to scattering, and the reflected light from surrounding terrain.

Call the top-of-atmosphere solar flux $E_{So}^{\downarrow}$: about $1367\,W\,m^{-2}$ during day, but zero at night. The direct solar beam at the surface ($E_{Sd}^{\downarrow}$) is a fraction of this, such that

$$E_{Sd}^{\downarrow} = E_{So}^{\downarrow} \cdot \cos Z \cdot \psi \qquad \text{with} \qquad \psi = \psi_o^{P/(P_o \cos Z)}. \tag{5.4}$$

Z is the zenith angle, the angular distance of the sun below a vertical line. Zenith angle varies with latitude (θ), time of year, and time of day (Oke 1987):

$$\cos Z = \sin\theta \sin\delta + \cos\theta \cos\delta \cos h, \tag{5.5}$$

in which δ signifies the solar declination, the angular distance between the sun and the equator. The hour angle, h, varies with the time of day such that $h = 0$ at local noon.

The parameter ψ, a number less than one, is the atmospheric transmissivity, a measure of the attenuation of the solar beam as it traverses the atmosphere (Oke 1987). Its value at sea level, ψ_o, is about 0.84 for a clear sky and 0.6 for thick haze. ψ_o decreases to zero under heavy

cloud cover, in which case only diffuse and reflected radiations contribute to insolation. The direct radiation on a glacier surface increases with altitude, because the thickness of atmosphere traversed by the solar beam decreases. This is why the ratio P/P_o appears in Eq. 5.4; P gives the atmospheric pressure at the glacier surface, and P_o the pressure at sea level (101.3 kPa). Conversely, a large zenith angle – a slanted solar beam – decreases the transmission because the beam must traverse a greater thickness of atmosphere.

For clear-sky conditions, solar radiation is limited primarily by its direct dependence on the zenith angle rather than by transmissivity. For example, measurements in clear-sky conditions at a site on the Greenland Ice Sheet ("ETH Camp" at 1155 m altitude, 69 °N) found an average value of about 0.8 for the transmissivity (Konzelmann and Ohmura 1995). In comparison, the mean daily value of $\cos Z$ in mid-summer at this latitude is about 0.4.

Figure 5.2 illustrates the annual cycle of $E^{\downarrow}_{Sd}$ at local noon, calculated from Eq. 5.4 for the complete range of latitudes, assuming a clear sky ($\psi_o = 0.84$) and a typical altitude for an extratropical glacier ($\approx$2500 m, or $P = 75$ kPa). The noon-time sun is, of course, much weaker at the poles than at low latitudes. In mid-summer, however, the daily total of flux (not shown) is about the same at all latitudes in the summer hemisphere because the length of day increases toward the poles.

Equation 5.4 applies to a horizontal surface. In general, corrections should be made for both slope and aspect; the zenith angle should be replaced by the angle between the solar beam and the normal to the local surface (Oke 1987). Surfaces that face the sun receive more direct radiation and ablate more rapidly than surfaces oriented obliquely to the sun's rays. On the other hand, in mountainous landscapes shadows eliminate all direct insolation at some times of the day, significantly reducing ablation – hence north-facing slopes are more heavily glaciated than south-facing slopes, in the northern hemisphere. Because of shading, small glaciers can survive in basins beneath steep mountain walls, even when glaciers have disappeared from everywhere else in the surrounding landscape.

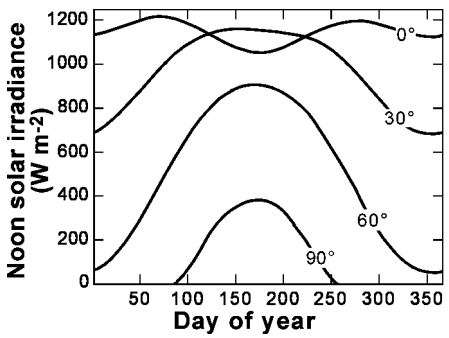

Figure 5.2: Peak daily (local noon) clear-sky direct solar radiation on a horizontal surface, as a function of latitude in the northern hemisphere. Curves were calculated from Eq. 5.4, with $P = 0.75$ bar and $\psi_o = 0.84$.

Diffuse radiation occurs in clear-sky conditions but matters most in cloudy conditions. Illumination from diffuse light explains why cloudy days are not completely dark. In clear-sky conditions at the ETH Camp in Greenland, the diffuse component was measured to be only 13–17 % of $E_S^{\downarrow}$ (Konzelmann and Ohmura 1995). Clouds greatly influence the summer average, however, and at this site the diffuse radiation was 40% of $E_S^{\downarrow}$ on average. At a cloudier, low-altitude, maritime ice cap in the South Shetland Islands, diffuse radiation accounted for about 60% of $E_S^{\downarrow}$ (Braun and Hock 2004). On cloudy days, the noon-time $E_S^{\downarrow}$ is often only 20% to 30% of its value under clear skies.

Solar radiation reflected from surrounding terrain can be significant in mountain regions, where reflective snow often mantles steep valley walls and peaks.

Summing the direct, diffuse, and reflected components gives the global radiation, $E_S^{\downarrow}$, the quantity of most interest to the energy budget. An effective transmissivity, ψ_*, expresses how much of the possible total solar radiation strikes the surface. Assuming a horizontal surface,

$$E_S^{\downarrow} = E_{So}^{\downarrow} \cdot \cos Z \cdot \psi_*. \tag{5.6}$$

The time-averaged value of ψ_* depends on the factors previously mentioned, such as cloud cover, altitude, and haze. Oerlemans and Knap (1998) determined monthly-mean values from continuous meteorological data collected at a site on the lower ablation zone of Morteratschgletscher, Switzerland. For summer months, ψ_* ranged from 0.44 to 0.59. Thus, at this mid-latitude alpine site about half of all the possible solar radiation reached the ground. At ETH Camp on the Greenland Ice Sheet, monthly means of ψ_* in summer are about 0.7 (Konzelmann and Ohmura, 1995).

5.3.2 Reflected Shortwave Radiation

The backscatter of shortwave radiation from snow and ice varies with wavelength, but the total reflected energy flux ($E_S^{\uparrow}$) can be described as a simple fraction of the downward flux. Define the *broadband surface albedo*, α_s, according to $E_S^{\uparrow} = \alpha_s E_S^{\downarrow}$. Common albedo values for snow and ice surfaces range from 0.2 to 0.85; the albedo therefore has a very large and important influence on the total shortwave radiation absorbed by the surface, $E_S^{\downarrow}[1-\alpha_s]$, and hence on ablation. Table 5.2 summarizes typical albedo values on glaciers.

Albedo at a site can be assessed by measuring the downward and upward solar radiation simultaneously, using radiometers that face up and down. Such data show the continuous variation of albedo over time. In the absence of direct measurements, albedo is often estimated from "typical" published values for snow or ice (e.g., Table 5.2; also Cutler and Munro, 1996). Most recent studies of glacier melt use parameterizations to estimate how the albedo varies through the melt season and from place to place (Oerlemans and Knap 1998; Brock et al. 2000).

Measurements reveal large variations of albedo over time on melting glaciers. Figure 5.3 illustrates how surface albedo changed through the melt season at a site near the equilibrium line

Table 5.2: Characteristic values for snow and ice albedo, from a literature review by S.J. Marshall.

Surface type	Recommended	Minimum	Maximum
Fresh dry snow	0.85	0.75	0.98
Old clean dry snow	0.80	0.70	0.85
Old clean wet snow	0.60	0.46	0.70
Old debris-rich dry snow	0.50	0.30	0.60
Old debris-rich wet snow	0.40	0.30	0.50
Clean firn	0.55	0.50	0.65
Debris-rich firn	0.30	0.15	0.40
Superimposed ice	0.65	0.63	0.66
Blue ice	0.64	0.60	0.65
Clean ice	0.35	0.30	0.46
Debris-rich ice	0.20	0.06	0.30

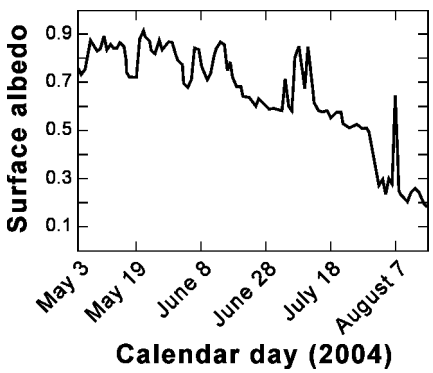

Figure 5.3: Variation of surface albedo in summer of 2004 at one location on Haig Glacier (data from Shea et al. 2005, courtesy of S.J. Marshall). Shown is the average mid-day (10:00–15:00) albedo, based on one-minute measurements by upward- and downward-looking radiometers. Rapid surface brightening (for example, on Aug. 6) occurs when new snow covers the surface. The transition from snow cover to bare glacier ice occurred July 28–30.

of a small glacier in the Canadian Rockies (Haig Glacier, 50.7 °N; Shea et al. 2005). The most profound change was the reduction of albedo, hence increased energy absorption, when the seasonal snow disappeared to reveal ice. Individual snowfall events brightened the surface and temporarily reduced absorption.

Fresh snow has an albedo of 0.8 to 0.9, and such high reflectivities are typical year-round in the interiors of polar ice sheets. After a snowfall, the albedo decreases over time, particularly during melting. Several processes are responsible. Snow metamorphism increases grain size,

which reduces the frequency of scattering at snow-air interfaces (Wiscombe and Warren 1980). Impurities such as rock particles and organic material concentrate on the surface, making the snow darker. Ponding of meltwater likewise increases absorption. Small quantities of water in the snow may also decrease albedo by effectively increasing the grain size (Warren 1982).

Snow albedo is very sensitive to particulate impurities; black carbon (soot) reduces albedo discernibly at concentrations of only about 0.1 ppm, and mineral dust does so at about 10 ppm (Warren and Wiscombe 1980). Natural snowpacks in tropical and mid-latitude areas often have impurity concentrations of this amount or greater (Thompson et al. 1979; Higuchi and Nagoshi 1977). Polar snowpacks are considerably more pure, with dust concentrations typically less than 0.1 ppm. On mid-latitude glacier snowpacks, the increasing concentration of impurities through the melt season reduces albedos to values as low as 0.3 by late summer.

Glacier ice typically has a lower albedo than snow, but, as Table 5.2 shows, ice albedos span a large range. Crystal size and bubble content influence albedo because they determine the amount and types of scattering surfaces in a unit volume of ice. Liquid water and impurities again increase absorption. The ice albedo varies from place to place in the ablation area; debris concentrates and water ponds in some areas; other areas are drained and flushed clean. On average, the ice exposed low in the ablation zone is the most absorptive – a consequence of high melt rates and long exposure times (Klok and Oerlemans 2002). Debris can be concentrated not just over a single melt season but cumulatively over many years.

Because albedos decrease over time in the melt season – on both snow and ice – the period of most effective energy absorption occurs later than the peak of insolation. Insolation is a maximum at the solstice (except in the tropics; Figure 5.2), but much of the winter snow still covers glaciers at this time. As the melt season progresses, darkening of the surface increases the absorbed or net shortwave radiation available for melt, $E_S^{\downarrow}[1-\alpha_s]$, by a factor of three to four. This is one reason why, on mid-latitude glaciers, peak melt rates occur one to two months after the solstice. (Warmer air in mid-summer also contributes.)

There are many factors not discussed here, and not usually addressed in energy balance studies, that further complicate shortwave absorption. For example, albedo depends on the angle of incidence of downward radiation. This means the albedo changes with time of day, with the proportions of direct and diffuse radiation, and with surface microtopography. Thin snowpacks are translucent, so the albedo depends partly on the underlying material. Sufficient accumulation of sediment on a glacier surface (typically more than a few centimeters in thickness) insulates the underlying ice and reduces melting. Snow and ice reflectivity vary as a function of wavelength, with greater reflection of visible wavelengths than near-infrared ones; the importance of all the effects just described should, in fact, vary with wavelength.

Wavelength-dependent processes also occur in the atmosphere. Visible wavelengths constitute a greater percentage of $E_S^{\downarrow}$ when skies are cloudy or humid, because water vapor and droplets preferentially absorb the near-infrared wavelengths. Given that the visible wavelengths are reflected more by the surface, the bulk albedo should therefore rise at the onset of humid or cloudy conditions.

5.3.3 Longwave Radiation

At infrared wavelengths, snow, ice, and liquid water emit as near-perfect radiators, with typical emissivities of $\epsilon_s = 0.94 - 0.99$. The emitted longwave radiation is thus, from Eq. 5.1,

$$E_L^{\uparrow} = -\epsilon_s \sigma T_s^4 \approx -\sigma T_s^4 \tag{5.7}$$

for surface temperature T_s. The negative sign indicates a loss of energy from the surface. For melting snow or ice, $T_s = 273.15$ K and $E_L^{\uparrow} = -315.6\,\mathrm{W\,m^{-2}}$. Within instrumental accuracy, this is the value measured by longwave radiometers in field studies (Greuell and Smeets 2001; Oerlemans and Klok 2002; Figure 5.4).

Downward longwave radiation $E_L^{\downarrow}$ originates as emissions from clouds and from atmospheric water vapor, carbon dioxide, ozone, methane, and other greenhouse gases. Such radiation is continually absorbed and emitted at different levels in the atmosphere. The flux at the surface depends on the amount and temperature of these constituents at different heights; longwave emissions originating throughout the bottom 1 km or so of the atmosphere reach the surface directly. The emissions are again governed by the relation $\epsilon \sigma T^4$, and so increase strongly with temperature in the lower atmosphere (Ohmura 2001). In contrast to the surface, however, the emissivity ϵ of the atmosphere deviates significantly from one, because the greenhouse gases absorb and emit only in certain wavelength bands.

The flux $E_L^{\downarrow}$ varies substantially and is difficult to predict without specific information about profiles of water vapor, clouds, and temperature in the lower troposphere. These data are seldom available, and $E_L^{\downarrow}$ must be measured or parameterized at a site. Most parameterizations define an effective atmospheric emissivity ϵ_a such that

$$E_L^{\downarrow} = \epsilon_a \sigma T_a^4, \tag{5.8}$$

for a near-surface air temperature T_a. With completely cloudy skies, $\epsilon_a \approx 0.95$ (Konzelmann et al. 1994). For clear skies with dry air, ϵ_a can be less than 0.5. As we will see next (Section 5.3.4) a value $\epsilon_a \approx 0.8$ is typical for a late-summer average. Hock (2005) discussed some of the parameterizations used in glaciology. Most calculate ϵ_a in terms of humidity and air temperature measured at 2 m above the surface. Though a crude way to account for the larger-scale atmospheric conditions governing $E_L^{\downarrow}$, this strategy is a reasonable one. Warm, humid conditions increase $E_L^{\downarrow}$, and heat the surface in periods of low cloud cover. Cold, dry conditions reduce $E_L^{\downarrow}$, and allow the surface to cool significantly at night. The parameterizations capture these first-order effects. Moreover, more than half of the downward longwave radiation originates within 100 m of the surface, according to theoretical calculations with radiation models (Ohmura 2001).

5.3.4 Field Example, Net Radiation Budget

Figure 5.4 shows measured shortwave and longwave radiation for two intervals in the month of August 2005, at 2650 m altitude (near the equilibrium line) on Haig Glacier, Alberta, Canada. (The glacier is described by Shea et al. 2005. Figures 5.3, 5.6, and 5.7 show more data from the

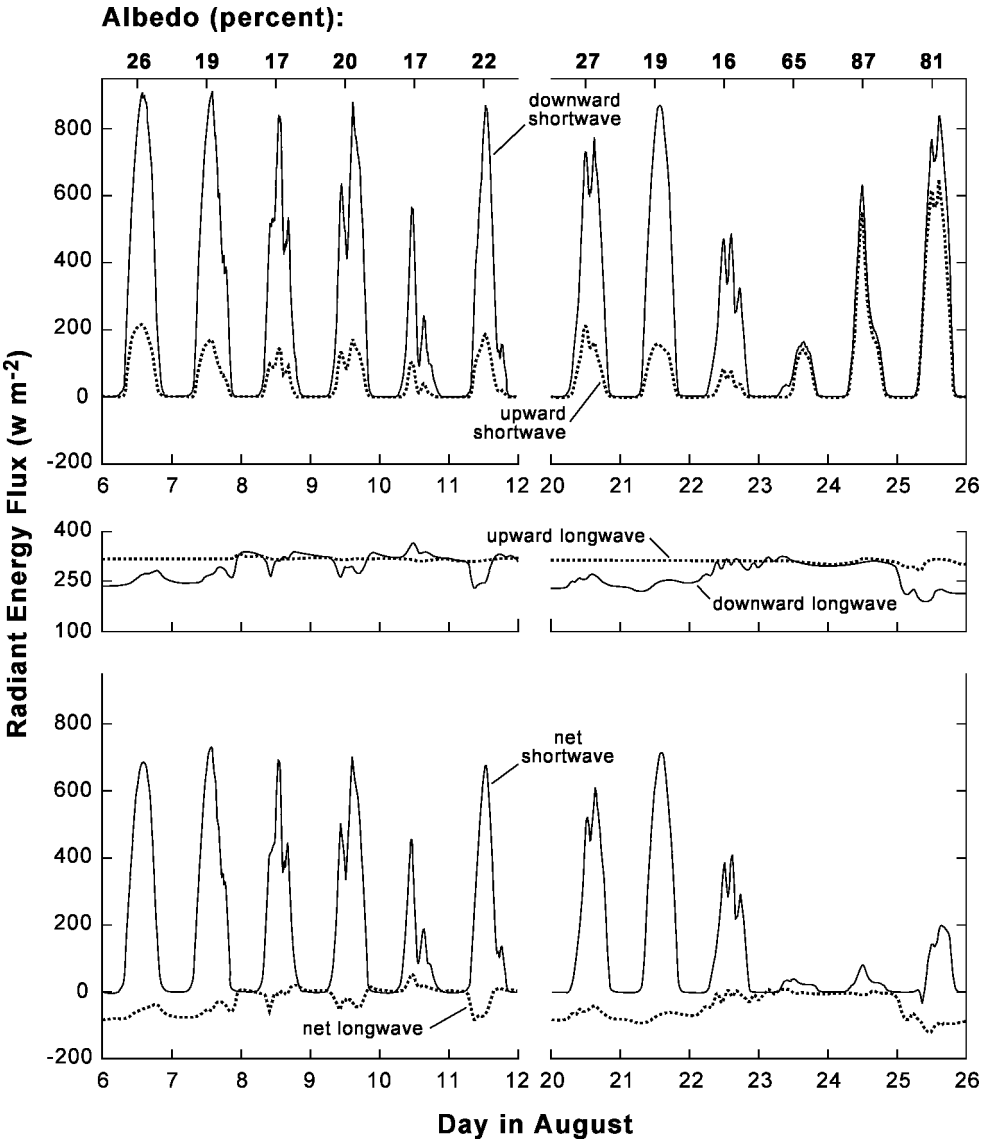

Figure 5.4: Measured radiative fluxes during two periods in August 2005, at one location on Haig Glacier. Data courtesy of S.J. Marshall. Numbers for each day above the top panel are mid-day albedos (percent).

same site.) Also shown is the net radiation $E_{\mathbf{R}}$,

$$E_{\mathbf{R}} = E_S^{\downarrow}[1-\alpha_s] + E_L^{\downarrow} - \left|E_L^{\uparrow}\right|. \tag{5.9}$$

We have smoothed the curves with a two-hour center-weighted filter; the original data are 10-second measurements. Daily values of surface albedo, indicated along the top of the figure, were calculated from mean mid-day measurements (hours 10:00–15:00). The variation of albedo at this site over a longer time period was shown in Figure 5.3.

At the beginning of both periods shown in the figure, the surface was glacier ice. The weather changed significantly during both. In the first interval, initially warm and clear conditions changed to cold and partly cloudy ones (beginning early on August 8), culminating with mostly cloudy conditions and a small snowfall on August 10. In the second interval, initially warm and clear conditions ended with a cooling and major snowfall event on August 23–24. This dramatically reduced the net solar radiation because of increased albedo. The net longwave radiation increased during cloudy and partly cloudy periods, despite colder near-surface air. Net radiation was generally positive and underwent diurnal variations, especially at times of low albedo.

The top row of Table 5.3 gives values averaged for the month; the other rows give minima and maxima. (The turbulent fluxes shown in the table are discussed later, in Section 5.3.6.) As reported from other glaciers, the largest single source of energy to the surface, averaged over days, was downward longwave radiation. The net flux of longwave, however, was usually negative, because the surface emitted the $315\,\mathrm{W\,m^{-2}}$ corresponding to irradiance at the melting temperature. Thus net shortwave radiation was the main source of energy for melt (sensible heat contributed about one-third as much). Averaged over days, the net longwave E_L^{Net} varied by about $100\,\mathrm{W\,m^{-2}}$ and so significantly affected the variations of the energy budget. Low values of $E_L^{\downarrow}$ corresponded with low relative humidity and low water vapor pressure. The correlation coefficients of $E_L^{\downarrow}$ with these two factors were $r = 0.59$ and 0.63, respectively. When relative humidities were close to 100%, downward and upward longwave fluxes essentially balanced. The effective atmospheric emissivity can be calculated as $\epsilon_a = E_L^{\downarrow}/\sigma T_a^4$, which gives an average for the month of $\overline{\epsilon}_a = 0.79$. The upward longwave varied little over the period because the surface temperature remained close to the melting point.

The melt production at this site will be discussed in Section 5.4.2.

5.3.5 Subsurface Conduction and Radiation

Both heat conduction and shortwave radiation can transfer energy through the bottom of the surface layer. These two processes give a net energy flux E_G, negative when directed downward, of

$$E_G = k_{\mathrm{T}} \frac{\partial T}{\partial z} - E_S^{\downarrow}[1-\alpha_s] \cdot f_\alpha(\Delta z). \tag{5.10}$$

Table 5.3: Mean and extreme energy budget terms ($\mathrm{W\,m^{-2}}$) for the month of August 2005, based on weather station measurements on Haig Glacier, Canada. (Data courtesy of S.J. Marshall.)

	α_s	$E_S^{\downarrow}$	E_S^{Net}	$E_L^{\downarrow}$	$E_L^{\uparrow}$	E_L^{Net}	E_{R}	E_H	E_E	E_N
Mean	0.42	217	121	270	−315	−45	76	37	−7	106
Minimum	0.12	0	0	187	−337	−123	−101	−27	−60	−151
Maximum	0.87	1101	892	384	−275	68	889	186	37	958

Conduction, the first term on the right, removes heat from the surface layer when it is warmer than the underlying ice. Here k_T is the thermal conductivity of snow or ice, and z is the depth below surface. With a subsurface temperature below the melting point, conduction produces daily gains and losses of heat from a shallow surface layer, decimeters in thickness. A thicker surface layer – several meters deep – gains and loses heat in the annual cycle. Negligible conductive heat transfer occurs if the ice or snow is all at its melting point. We discuss conductive heat transfer and variations of subsurface temperatures in detail in Chapter 9.

Much of the shortwave radiation penetrating snow or ice scatters from the surfaces of grain boundaries, fractures, and bubbles, and becomes the reflected flux $E_S^{\uparrow}$ discussed in Section 5.3.2. The remaining flux, of magnitude $E_S^{\downarrow}[1-\alpha_s]$, is absorbed. Most of the absorption occurs close to the snow/ice surface, but its distribution with depth depends on the scattering and absorption of different wavelengths. The multiplier f_α, in the second term on the right side of Eq. 5.10, declines rapidly from one at the surface to near zero not far below. Its value depends on the chosen thickness Δz of the surface layer. Of the total absorbed shortwave radiant energy, a fraction $[1-f_\alpha]$ heats or melts the surface layer directly, while the remaining fraction heats or melts the layers beneath (some of it may return to the surface layer by conduction). This distinction is important only if temperatures beneath the surface are subfreezing; to calculate the total melt in temperate ice or firn, we need to choose a large enough Δz to make $f_\alpha = 0$.

The depth to which any significant absorption occurs is apparently a few millimeters in snow, a few centimeters in ice with abundant bubbles, and as much as 20 cm in "blue ice" with fewer bubbles (Brandt and Warren 1993; Bintanja et al. 1997). Water pockets and rock particles, however, can increase absorption at depth. In cold, dry places with ice surfaces, as in parts of Antarctica, the shortwave absorption at depth is a small but nontrivial part of the energy budget (Bintanja et al. 1997; Bintanja 2000).

5.3.5.1 Why Does Glacier Ice Look Blue or White?

The focussing of absorption near the surface does not imply complete darkness at greater depths; some radiation penetrates to a few tens of meters but then mostly scatters back to the surface and contributes to the surface albedo rather than to absorption. The total down-welling radiative flux in the subsurface, $E_z^{\downarrow}$, declines with depth z:

$$E_z^{\downarrow} = E_S^{\downarrow} \cdot \exp\left(-\chi\,\ell(z)\right). \tag{5.11}$$

The depth of penetration depends on the the extinction coefficient, χ, and the path length, ℓ, a measure of how much ice the radiation travels through. Extinction includes both scattering and absorption, and ℓ increases in proportion to both depth and density and varies with incidence angle.

Absorption within ice depends strongly on wavelength (Figure 5.5). If a beam of shortwave radiation shines into solid ice, the near-infrared wavelengths are absorbed near the surface (within

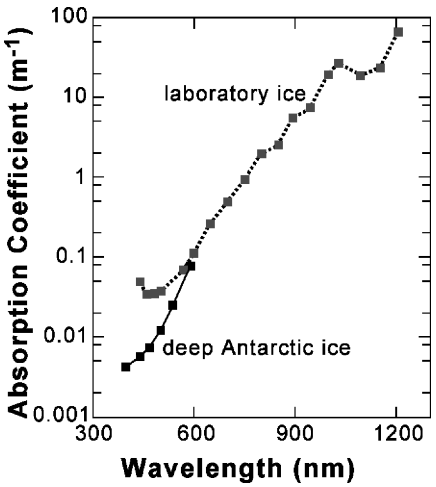

Figure 5.5: Measured absorption coefficient in pure ice, as a function of wavelength. The intensity of a beam of light shining through ice decreases with distance z, in proportion to $\exp(-\chi z)$: the extinction coefficient χ equals the absorption coefficient if there is no scattering. Laboratory measurements are those of Grenfell and Perovich (1981). The coefficient for "deep Antarctic ice" was determined by transmission of light between detectors frozen into boreholes in the bubble-free ice beneath South Pole, Antarctica (data from Askebjer et al. 1997). At the smallest wavelengths, the laboratory measurements overestimate the absorption, most likely due to scattering from microscopic fractures in the laboratory-prepared ice.

centimeters to decimeters), whereas visible wavelengths penetrate much farther. The penetration distance of visible light is inversely related to wavelength. Blue light travels several orders of magnitude farther than the near-infrared radiation (Askebjer et al. 1997). Light scattered from depths of several meters or more within a block of ice is therefore blue; this accounts for the renowned blue hue of glacial ice. In ice with abundant bubbles or other scattering surfaces, however, reflection occurs near the surface and the reflected light is still white.

5.3.6 Turbulent Fluxes

As winds flow along the surface of a glacier, turbulent eddies mix the air vertically. The temperature of the air adjacent to the glacier surface (the *skin temperature*) equals the temperature of the ice or snow. If the overlying air (the *lower boundary layer* or *surface layer*) is warmer than the surface, the mixing transfers sensible heat to the surface, at rate per unit area E_H. The moisture content of the air at the surface is determined by the saturation vapor pressure and hence the skin temperature (Eqs. 4.4 and 4.5). In the presence of drier overlying air, mixing transfers moisture away from the surface. The surface must evaporate or sublimate to maintain saturation of the air adjacent to it. This consumes latent heat, at rate per unit area E_E. In general, both of these fluxes can be either positive or negative.

5.3.6.1 Bulk Aerodynamic Approach

From the preceding description it is sensible (so to speak) to conclude that the energy fluxes E_E and E_H are roughly proportional to the contrasts of moisture and temperature between the surface and the overlying air. Call the contrasts $T_a - T_s$ and $q_a - q_s$; here T_a and T_s stand for temperatures of the lower boundary layer and the surface, and q_a and q_s stand for the corresponding absolute humidities (mass of water vapor per unit volume). Fluxes also increase with the strength of vertical turbulent exchange, an increasing function of the frequency of eddies and their distance of propagation. In bulk, the turbulent exchange of air relates to three factors; how fast the air flows (measured by the wind speed u a few meters above the surface), how rough the surface is, and whether buoyancy stabilizes the air against vertical mixing or not ("stability"). Of these, the wind speed is the most important. Thus, defining two coefficients, C_{H} and C_{E}, as the *bulk exchange parameters* for heat and moisture, a first approximation takes the form:

$$E_H = \rho_a c_a C_{\mathrm{H}}\, u\, [T_a - T_s] \tag{5.12}$$

$$E_E = \rho_a L_{v/s} C_{\mathrm{E}}\, u\, [q_a - q_s] \tag{5.13}$$

with ρ_a the density of air, c_a its specific heat capacity at constant pressure, and $L_{v/s}$ the latent heat of vaporization or sublimation. Using Eqs. 5.12 and 5.13 is referred to as the "bulk aerodynamic approach," because u, T_a, and q_a are regarded as representative values for the lower boundary layer, assumed to be thoroughly mixed (Garratt, 1992). In fact, all of these parameters vary with height, so the values for the exchange parameters must depend on the height at which measurements are made (Oerlemans and Klok 2002). To find values of the coefficients, for a given height, we next combine an approximate model of the turbulence with empirical constraints; this is the goal of the next four sections. Such an analysis also highlights some of the limitations of the approach.

5.3.6.2 Fluxes of Heat and Vapor: Flux-gradient Theory

Heat transfer by turbulent convection is viewed as analogous to conduction, with eddies playing the part of molecules. The vertical flux of heat E_H is therefore taken proportional to the vertical temperature gradient $\partial T/\partial z$ (with z increasing upward) and to a coefficient specifying the effectiveness of the transfer process, known as the *eddy diffusivity for heat*, K_h:

$$E_H = K_h \rho_a c_a \frac{\partial T}{\partial z}. \tag{5.14}$$

Because turbulent convection greatly exceeds molecular conduction, K_h is roughly a factor of 10^5 larger than the thermal diffusivity of air at rest. The coefficient K_h varies with height z. In periods of melting, the fixed surface temperature implies that $\partial T/\partial z$ and hence E_H increase with the air temperature in excess of 0 °C, as in Eq. 5.12.

The vertical flux of vapor can be treated similarly. The amount of heat per unit volume, $\rho_a c_a T$, is replaced by the humidity q, the mass of water vapor per unit volume. The upward vapor flux (per unit area), Q_w, is

$$Q_w = -K_w \frac{\partial q}{\partial z}, \tag{5.15}$$

with K_w the *eddy diffusivity for water vapor*. The energy lost from the surface then amounts to $E_E = -L_{v/s} Q_w$. The most useful way forward involves rewriting this equation in terms of the water vapor pressure e rather than q, because we can calculate e as a function of temperature for the saturated air at the surface. From the gas law,

$$q = M_w \frac{e}{RT}, \tag{5.16}$$

where M_w is the molecular weight of water and R the gas constant. Further, the gas law gives an expression for RT in terms of the total pressure P,

$$\frac{P M_a}{\rho_a} = RT, \tag{5.17}$$

with M_a the molecular weight of air. It follows that

$$q = \frac{M_w}{M_a} \frac{\rho_a e}{P} = 0.622 \frac{\rho_a e}{P} \tag{5.18}$$

and so

$$E_E = \rho_a K_w L_{v/s} \frac{0.622}{P} \frac{\partial e}{\partial z}. \tag{5.19}$$

The pressure of water vapor in saturated air at the surface is $e = 611$ Pa. If the lower boundary layer has a comparatively small vapor pressure, the surface loses ice to evaporation and sublimation. The vapor pressure in the boundary layer increases with both temperature and relative humidity. In summer, air temperatures below 0 °C favor evaporation and sublimation; those above favor condensation. Dry air strongly favors evaporation and sublimation, however, so relative humidity is often the most important factor. Note that the air at the surface is not always saturated, as assumed; the preceding formulation therefore systematically underestimates direct condensation (Box and Steffen 2001).

5.3.6.3 Turbulence and Flow of the Air

The turbulence of the air is measured by the *eddy viscosity*, K_m, defined by the equation

$$\tau = \rho_a K_m \frac{\partial u}{\partial z}. \tag{5.20}$$

Here τ denotes the shear stress acting on the surface and in the air above, and u indicates the wind speed at height z. This relation is equivalent to the constitutive rule of a fluid of kinematic viscosity K_m. This equation resembles those for moisture and heat fluxes; the shear stress can be regarded as a vertical flux of horizontal momentum.

Theoretical and experimental results both suggest that although K_m varies with height z the shear stress τ does not, at least in the first few meters above a horizontal surface. Equation 5.20 then implies that

$$K_m \frac{\partial u}{\partial z} = \frac{\tau}{\rho_a} = \text{constant}. \tag{5.21}$$

The quantity $[\tau/\rho_a]^{1/2}$ has the dimensions of velocity, and is known as *friction velocity*, denoted u_*. Measurements have shown that, in the first few meters above the surface, the wind speed u typically varies as the logarithm of the height and scales with u_*, so that:

$$u(z) = \frac{1}{k_o} u_* \ln\left(\frac{z}{z_0}\right). \tag{5.22}$$

k_o is a dimensionless constant, *von Kármán's constant*, with a value of 0.4; z_0 is the *surface roughness parameter*, with units of length (and often simply called "roughness"). This small quantity represents the height above the mean surface at which the wind speed is nominally zero. Its value can be determined from measurements of wind speed at several heights above the surface, using Eq. 5.22. Table 5.4 gives typical values, taken from a compilation by Brock et al. (2006).

The roughness z_0 is generally proportional to the height of bumps and undulations on the surface, but typically smaller than 5% of their amplitude. With z_0 determined, a value of u_* can be obtained using Eq. 5.22 and additional measurements of wind speed. Typical values of u_* for melting glacier surfaces are in the range 0.1 to 0.5 $\mathrm{m\,s^{-1}}$ (Kuhn 1979). Finally, Eq. 5.22 can be differentiated to show that $\partial u/\partial z = u_*/k_o z$; combining this with Eq. 5.21 gives an expression

Table 5.4: Typical ranges of surface roughness parameter in millimeters (Brock et al. 2006).

Smooth ice	0.01–0.1
New snow and polar snow	0.05–1
Snow on low-latitude glaciers	1–5
Ice in ablation zone	1–5
Coarse snow with sastrugi	11
Penitentes[†]	30
Rough glacier ice	20–80

[†] Pinnacles and blades of snow.

for the eddy viscosity,

$$K_m = u_* k_0 z. \tag{5.23}$$

Eddy viscosity thus increases with the strength of the wind (u_*); faster wind increases the vigor of turbulent mixing. The turbulent energy fluxes, E_H and E_E, should therefore also increase with u_*.

5.3.6.4 Flux-Gradient Methods for Determining Energy Fluxes

There is some evidence that, at any given height, the three eddy viscosities K_m, K_h, and K_w are approximately equal in an atmosphere with near-neutral stability. (A neutral atmosphere is one in which the temperature gradient equals the dry adiabatic lapse rate, approximately 1 K per 100 m. The assumption of equal eddy viscosities is, in any case, only plausible if wind speed, temperature, and vapor pressure all vary as the logarithm of height). By taking $K_m = K_h = K_w$, Eqs. 5.14 and 5.19 can give values for the turbulent fluxes, if combined with measurements of temperature and vapor pressure at various heights, and a value for K_m determined from wind speed measurements and Eq. 5.23. The measurements are made by instruments mounted at different levels on a mast of several meters' height.

The atmosphere above a glacier is often far from neutral. Temperature increases of 8 degrees in the first 2 meters have been measured (Holmgren 1971, Part B). Such a strong temperature inversion implies an extremely stable atmosphere and hence reduced turbulence. Grainger and Lister (1966) reviewed different laws of wind-speed variation with height and compared them with field observations. They concluded that the logarithmic law is best not only for neutral but also for extremely stable atmospheres.

How much error is introduced by assuming equality of the three eddy viscosities is unclear. Recent reviews of available data conclude that the the assumption $K_m = K_h$ is reasonable for stable boundary layers (Andreas 2002).

5.3.6.5 Calculations Using Transfer Coefficients

The flux-gradient theory can be used to formulate the bulk aerodynamic relations (Eqs. 5.12 and 5.13) into a usable form. From Eqs. 5.14 and 5.23 and the assumption $K_h = K_m$,

$$E_H = \rho_a c_a k_o u_* z \frac{\partial T}{\partial z}. \tag{5.24}$$

Integration gives

$$E_H = \rho_a c_a k_o u_* \frac{T - T_s}{\ln(z/z_0)} \tag{5.25}$$

for surface temperature T_s. Substitution for u_* from Eq. 5.22 gives

$$E_H = \rho_a c_a C^* u\,[T - T_s] \quad \text{with} \quad C^* = \frac{k_o^2}{\ln^2(z/z_0)}. \tag{5.26}$$

The dimensionless parameter C^* is called the *transfer coefficient*. The density of air, $\rho_a = \rho_a^\circ P/P_0$, depends on atmospheric pressure P; with ρ_a° being the density at standard pressure P_0. Substitution of numerical values $\rho_a^\circ = 1.29\,\mathrm{kg\,m^{-3}}$, $P_0 = 1.013 \times 10^5$ Pa, and $c_a = 1010\,\mathrm{J\,kg^{-1}K^{-1}}$ gives

$$E_H = 0.0129 C^* P u(z)\,[T(z) - T_s]\,. \tag{5.27}$$

This equation can be used with values for u and T measured at a known height z above the ground. Daily means are commonly used; in some cases they are values from weather stations nearby, adjusted for differences in elevation, rather than measurements on the glacier. This equation is normally applied to melting surfaces, in which case $T_s = 0\,^\circ\mathrm{C}$.

Equation 5.19, with the assumption $K_w = K_m$, leads to a similar relation for the latent heat flux

$$E_E = 0.622 \rho_a^\circ L_v C^* u(z)\,[e(z) - e_s]\,/P_0 = 22.2 C^* v\,[e - e_s] \tag{5.28}$$

involving the vapor pressures above and at the surface, e and e_s. The former is measured, the latter calculated by assuming saturation.

The value of C^* will depend on measurement height and surface roughness, but not strongly. For a measurement height z of 1 to 2 m, the values of z_0 in Table 5.4, and $k_o = 0.4$, Eq. 5.26 gives values of C^* in the range 0.002 to 0.004 for melting snow and ice surfaces. Table 5.5 lists some published values, all reduced to this dimensionless form.

The data in this table suggest that values for C^* of 0.0015 for snow and 0.002 for ice are appropriate. The value of C^* is not very sensitive to variations in roughness; increasing z_o from 1 mm to 1 cm increases the transfer coefficient by a factor of two. Using the value $C^* = 0.002$ in Eq. 5.27 suggests that, with typical conditions ($P = 80\,\mathrm{kPa}$, $u = 5\,\mathrm{m\,s^{-1}}$), air at 5 °C provides a sensible heat flux of about $50\,\mathrm{W\,m^{-2}}$ to a melting surface. With $e/e_s = 0.8$ and the same wind speed, the latent heat flux removes about $25\,\mathrm{W\,m^{-2}}$ from the surface.

Table 5.5: Transfer coefficients C^* for melting snow and ice surfaces.

Surface	1000 C^*		Reference
	Heat	Vapor	
Snow	1.66	2.04	Holmgren 1971, Part D
Snow/ice	2.0	2.0	Hogg et al. 1982
Snow	1.3	1.5	Ambach and Kirchlechner 1986
Ice	1.5	1.5	Oerlemans and Klok 2002
Ice	1.9	2.2	Ambach and Kirchlechner 1986
Ice	3.9	3.9	Hay and Fitzharris 1988

5.3.6.6 Further Comments on the Turbulent Fluxes

1. The height at which air temperature equals the skin temperature is not necessarily the same as the height z_0 (Andreas 1987, 2002). In particular, microtopography of the surface should not constrain the transfer of heat as much as the transfer of momentum. Thus the lower limit of the integration leading to Eq. 5.25 should perhaps be some other number, z_0', smaller than z_0. The definition of the transfer coefficient then would include $\ln(z/z_0)\ln(z/z_0')$ in its denominator, rather than $\ln^2(z/z_0)$, giving a smaller transfer coefficient C^*. Hock and Holmgren (2005) argued that z_0' for glacier surfaces is typically only $0.01 z_0$. If $z_0 = 3\,\text{mm}$, this implies a 40% reduction in C^* for $z = 2\,\text{m}$. Andreas (2002) reviewed evidence that z_0/z_0' depends on the surface roughness and wind speed; the transfer coefficient apparently varies, again, within a factor of two. These arguments also apply to the transfer coefficient for latent heat.

2. Turbulent exchanges depend on the stability of the lower boundary layer. If the temperature decreases with height more rapidly than the adiabatic lapse rate (i.e., an unusually warm surface compared with the air above), buoyancy enhances vertical mixing. The usual situation on glaciers in summer is the opposite; the cold, dense air at the surface suppresses vertical mixing ("stable conditions"). In stable conditions, the wind shear $\partial u/\partial z$ concentrates near the surface more than implied by Eq. 5.22. Applying stability corrections to calculations of E_H and E_E requires a large number of theoretical assumptions, and does not appear justified for glaciers, given the sparse measurement constraints and the complexity of the surfaces (Holmgren 1971, part B; Munro 1989; Hock and Holmgren 1995; Braithwaite 1995; Oerlemans and Klok 2002). The surface roughness on most glaciers varies significantly over distances of only tens of meters; the wind profile is thus not adjusted to the underlying surface (Oerlemans 2001, p. 33). Nonetheless, it is now common practice to apply a stability correction based on the theory of Monin and Obukhov (1954) (see Stull 1988).

3. Although a logarithmic wind profile (Eq. 5.22) may be a good approximation close to the surface, many observations on glaciers show that the wind speed attains a maximum at a height of several meters above the surface (Smeets et al. 1999; Oerlemans and Grisogno 2002). This is typical of the "glacier wind," a down-slope flow of cold, dense air (Oerlemans 2001, pp. 34–38).

4. Box and Steffen (2001) measured surface vapor fluxes at a number of sites on the Greenland Ice Sheet, using several different methods. The authors concluded that a flux-gradient method using measurements from two heights more accurately gauges downward water vapor flux than does the one-height method. On the other hand, in some situations calculations with the one-height method are significantly less sensitive to measurement errors (Bintanja and van den Broeke 1995).

The formulation outlined here, using transfer coefficients, captures the essential features of the turbulent exchange processes. Quantitatively, however, the method is only accurate to within

a multiple of a few, unless site-specific calibrations are applied. All methods for determining turbulent fluxes rely on gross simplifications of the fluctuating mass and heat flows near the surface; calibration is a necessity for quantitative accuracy.

5.3.6.7 Field Example of Turbulent Fluxes

Figure 5.6 shows meteorological variables and the turbulent energy fluxes for two intervals in the month of August 2005 on a mid-latitude mountain glacier: the same location and time period as shown in Figure 5.4. The onset of cool conditions on both August 8 and 23 significantly reduced

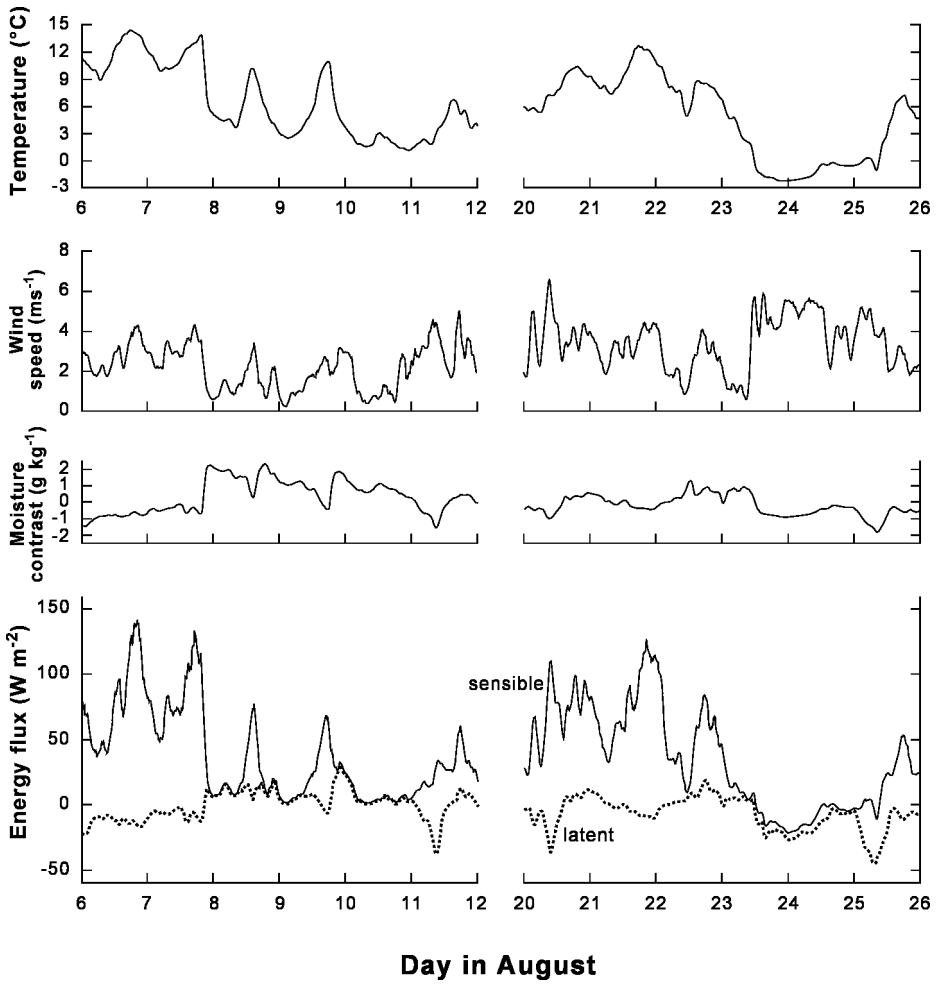

Figure 5.6: Inferred turbulent energy fluxes during two periods in August 2005, at one location on Haig Glacier (bottom panel). Top three panels show meteorologic conditions: air temperature and wind speed at 2 m height, and depression of water vapor content at 2 m height relative to water vapor content at the surface (relative humidity was measured at 2 m; saturation was assumed at the surface). Data and calculations courtesy of S.J. Marshall.

the sensible heat flux. The latent heat fluxes were relatively small. These calculations used the transfer coefficient method with a roughness of $z_0 = 3\,\text{mm}$, and $z_0' = 0.01 z_0$ for both sensible and latent heats (see item 1 in the preceding list).

Table 5.3 gives the mean fluxes for the month. Sensible heat flux was a significant source of energy to the glacier, about half as large as net radiation, whereas sublimation and evaporation were a minor energy sink. The energy fluxes varied over time primarily because of changes in the driving variables (the temperature and humidity differences, $T_a - T_s$ and $q_a - q_s$) rather than wind speed. Applying a stability correction (see item 2 in the preceding list) using the formulation of Holtslag and de Bruin (1988), reduced the the calculated energy fluxes by about 20%.

5.3.6.8 Rate of Ablation by Sublimation

Sublimation strips material from the surface at a rate (thickness per unit time)

$$\dot{s} = -E_E / \rho L_s \tag{5.29}$$

for surface density ρ. With reference to Eq. 5.28, three processes favor sublimation: dry air (small e), a warm surface (large e_s), and strong winds (large u).

Generally, the energy consumed by evaporation and sublimation reduces the energy available for warming and melting the surface. In Greenland, the annual reduction of melt is small but not trivial. In their analysis of Greenland Ice Sheet surface balance, Box and Steffen (2001) concluded, in agreement with earlier investigators, that the energy sink from sublimation and evaporation has an important role in maintaining the ice sheet. It is also a major factor on high-altitude glaciers (Section 5.4.5.3).

5.4 Relation of Ablation to Climate

5.4.1 Calculating Melt from Energy Budget Measurements

The amount of ice melted in a given time period is controlled by the net vertical energy flux (E_N) according to Eqs. 5.2 and 5.3, integrated over time. E_N needs to be modelled to answer many questions about how glacier mass balance depends on climate and other factors. One approach uses measurements or model values for each of the separate energy fluxes that sum to E_N. In principle, this approach is the best way to rigorously connect glacier ablation to climate processes. In practice, the uncertainties in such a method can be large. To determine the accuracy requires comparisons to measurements of the melt itself. Detailed energy budget studies have now been made on many glaciers worldwide.

Figure 5.7 illustrates melt and energy fluxes for the month of August 2005 at Haig Glacier, Canada (see Figures 5.4 and 5.6 for the radiative and turbulent fluxes in two intervals within this month). The model melt rates shown here are daily values, calculated by integrating the E_N over each day, but only using times with surface temperature at 0 °C. For comparison, the

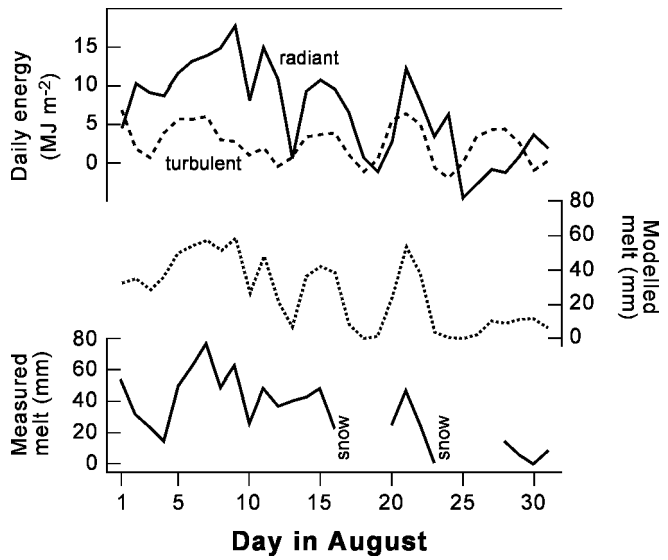

Figure 5.7: Daily-total melt parameters for the month of August 2005, at Haig Glacier. Top panel shows the net values of radiant and turbulent fluxes, integrated over each day. The sum gives a net energy flux that is converted to modelled melt (middle panel), using Eq. 5.3, when temperature is at melting point. The inferred net energy flux can be compared to actual melt, determined from surface deflation measured with a sonic ranger (bottom panel). Significant new accumulations of snow occurred at the two times labelled "snow." Subsequent compaction of the snow made it impossible to determine the melt from surface deflation; we have assumed this effect lasts for two days after snowfall ends. Data and calculations courtesy of S.J. Marshall.

measured melt rates were determined from observations of the rate of surface lowering, obtained with a sonic ranger. No values are shown during snowfalls and for two days after because snow density was not measured. The modeled and measured melt rates compare well; observed melt totalled 89 mm (w.eq.), compared to a model value of 81 mm (an integrated E_N of 284 MJ m^{-2}). Daily values correlated moderately well ($r = 0.79$). Net radiation caused more melt than did the turbulent fluxes, but both contributed to variations.

Hogg et al. (1982) made a similar comparison using data from Hodges Glacier, South Georgia. They measured downward and upward shortwave radiation and net total radiation and calculated turbulent fluxes by the transfer-coefficient method from daily mean temperatures, water vapor pressures, and wind speeds measured at one point on the glacier. The total ablation calculated from the energy fluxes was 3.45 m of water, which compared well with the 3.37 m measured at ablation stakes. Again, Braithwaite and Olesen (1990) made the comparison at two sites near the margin of the ice sheet in West Greenland. In this study, the fluxes were less constrained by measurements. Downward shortwave radiation was measured but values of albedo were assumed. Upward longwave radiation was calculated from Eq. 5.7, but downward longwave was estimated from air temperature and cloudiness using an empirical relation. Turbulent

fluxes were computed using Ambach and Kirchlechner's transfer coefficients (Table 5.5). The calculated ablation rates for the season were within 1 mm day^{-1} of the observed values, although the standard deviations of the daily discrepancies at the two sites were 14 and 19 mm day^{-1}.

These results, and others, suggest that energy budgets calculated from relatively simple observations can provide reliable estimates of ablation rates, in spite of the difficulties in measuring the net radiation and the simplifying assumptions in the theories for turbulent fluxes.

It is considerably more difficult to calculate ablation for a whole glacier than for a few sites with meteorological measurements. Many of the important variables (wind, humidity, surface roughness, cloudiness, surface albedo) vary significantly from place to place and over time. Nonetheless, spatially distributed energy balance calculations have been applied to some intensively studied glaciers and appear to work well (Arnold et al. 1996; Klok and Oerlemans 2002; Hock and Holmgren 2005). So too for the Greenland Ice Sheet (Box et al. 2004, 2006). But in most studies, especially of large regions and of long-term changes, constraints from measurements are sparse, and simplified approaches must be used; we discuss these next.

5.4.2 Simple Approaches to Modelling Melt

Empirical regression equations relating measured ablation rates to air temperatures – and other variables measured by weather stations – provide a simple alternative to energy-budget calculations. The weather stations may be on the glacier or nearby. Such equations have several uses, including extending series of annual ablation measurements backward in time, estimating ablation on glaciers without measurements, and predicting the increase of ablation rate with warming. The results from these analyses need to be regarded as uncertain approximations. Ideally, uncertainties can be assessed from constraints on all the components of the energy budget. In practice, such an assessment is seldom feasible.

The most obvious variables to use in a simple melt relation are the air temperature and the radiation. The first variable is connected to the sensible heat flux, to whether the surface is warm enough to melt, and, in some complicated fashion, to the downward longwave radiation. For the second variable, either net total radiation or net solar radiation might be used.

Braithwaite (1981) used data from four energy-budget studies on two glaciers in Arctic Canada to discern correlations. He found that daily ablation correlated with air temperature but not with net radiation. This was because air temperature, in turn, correlated with the sensible heat flux, which varied more than the net radiation. Nonetheless, variations in air temperature accounted for only half the variance of ablation rate. Thus, although air temperature predicted ablation better than did net radiation, it was not a particularly good predictor at the timescale of days.

A more important question is whether simple relations can make good predictions of total ablation over a year. In this case, the mean annual temperature might be a poor indicator of melt because the ablation season lasts only a few months and the temperature during the rest of the year has little relevance. Mean summer temperature is a better choice. On climatic timescales

of decades and longer, however, means of summer and annual temperature are likely to vary together.

In one analysis of year-to-year variability, Hanson (1987) obtained a correlation coefficient of −0.93 between the annual mass balance measured along a flow line on Barnes Ice Cap, Canada, and the mean summer temperature measured at a weather station 120 km away. At this ice cap, precipitation varies little from year to year and mass balance variations depend almost entirely on the summer ablation. In another case, Braithwaite and Olesen (1989) used 6 years of data from Nordbogletscher, South Greenland. They obtained a correlation with mean summer temperature of 0.84. The correlation with mean annual temperature was 0.56 and not statistically significant. These results are surprisingly good considering the simplicity of the climate metrics compared to the complexity of controls on the energy budget.

5.4.2.1 Positive Degree Days

In principle, ablation should relate yet more closely to an index that accounts not only for mean summer temperature but also for the amount of time that air temperatures exceed 0 °C. Only during such conditions will the sensible heat flux contribute directly to melt. Moreover, melt of the surface may cease entirely if air temperatures fall below 0 °C for an extended period. The most commonly used index is *positive degree days*, which we symbolize D (Krenke and Khodakov 1966; Braithwaite and Olesen 1989; Huybrechts et al. 1991; Jóhanesson et al. 1995). This index is defined, for time period Δt measured in days, as

$$D(\Delta t) = \int_{\Delta t} T_C \, H(T_C) \, dt \quad \text{with} \quad H(T_C) = \begin{cases} 1 & \text{if} \quad T_C > 0 \\ 0 & \text{if} \quad T_C < 0 \end{cases} \tag{5.30}$$

where T_C signifies the Celsius temperature of the air. A common approach is to calculate D using daily mean temperatures, in which case $D = \sum_j \overline{T}_{cj} H_j$, the sum for all days j in the time interval of interest. The D index is often symbolized PDD in the literature, an awkward notation for equations.

D provides a rough approximation of the integrated heat energy driving melt over the time interval of interest. For application in models, the total surface melt m_s over time Δt is parameterized simply as

$$m_s = f_m D, \tag{5.31}$$

in which f_m denotes the *degree-day melt factor*, an empirically determined coefficient relating D to observed melt. Equation 5.31 is equivalent to assuming that, during periods of melt,

$$\int_{\Delta t} E_N \, dt = \rho_w L_f f_m D(\Delta t). \tag{5.32}$$

Thus f_m should be larger for an ice surface than a snow surface, since the smaller albedo of ice results in greater net energy in otherwise similar conditions. Numerous measurements do show that ice surfaces ablate more rapidly than snow surfaces (e.g., Hoinkes and Steinacher 1975). Based on observations in Greenland (e.g., Braithwaite and Zhang 2000), values of f_m for snow and ice of, respectively, $f_{ms} = 3$ and $f_{mi} = 8\,\mathrm{mm\,day^{-1}\,^{\circ}C^{-1}}$ are typically used in ice sheet models. For the full month of observations at Haig Glacier shown in Figure 5.7, D was 179.5 day–°C, and hence $f_m \approx 5\,\mathrm{mm\,day^{-1}\,^{\circ}C^{-1}}$. When modelling a large region, such as the Greenland Ice Sheet, different f_m values need to be used for different regions, not only because of different surface albedos but also because the contribution of turbulent fluxes to total melt varies with such factors as wind speed (Lefebre et al. 2005). For summer totals, a common approach is to calculate degree days separately for the periods of snow cover (D_s) and exposed ice (D_i), and then the total melt as $m_s = f_{ms} D_s + f_{mi} D_i$.

In their six-year study of Nordbogletscher, Braithwaite and Olesen (1989) obtained a correlation coefficient of 0.96 between annual ice ablation and D, corrected for snow accumulation. Thus, compared to mean summer temperature, positive degree days explained about 20% more of the variance of ablation. Several other studies confirm a strong relation between ablation and D in Greenland in summer months (Figure 5.8). In general, D seems to act as a better proxy for ablation than expected from a detailed understanding of the physics; we consider the underlying reasons in the next section.

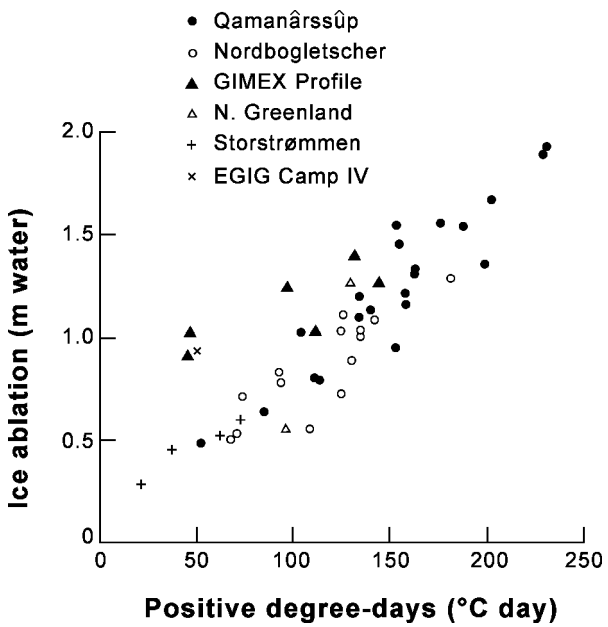

Figure 5.8: Correlation of measured ice ablation (standardized to one month) with positive degree days, in six regions of the Greenland Ice Sheet margin. Redrawn from Braithwaite (1995).

Degree-day melt models may be improved by using separate parameterizations for the influence of degree days and the influence of downward shortwave radiation (e.g., Cazorzi and Dalla Fontana 1996; Hock 1999). For example, we might write the melt in time Δt as $m_s = f_m D(\Delta t) + g_m \int_{\Delta t} E_S^{\downarrow} dt$, with g_m being a radiation-melt index that varies spatially and temporally as a function of albedo. A related approach is to use Eq. 5.31 but to make f_m an explicit function of both $E_S^{\downarrow}$ and surface albedo.

5.4.3 Increase of Ablation with Warming

The response of glaciers to climate change depends critically on how much the annual ablation increases as the climate warms. This depends on many factors, but simple analyses give useful approximations.

When Braithwaite (1981) examined the correlation of daily ablation rates with air temperatures on glaciers in Arctic Canada, he obtained an average sensitivity of $6.3\,\mathrm{mm\,day^{-1}\,°C^{-1}}$. Earlier published values were in the range 4.5 to $7\,\mathrm{mm\,day^{-1}\,°C^{-1}}$ (Braithwaite 1980). It is not obvious that these numbers, derived from daily variations, should be relevant to total ablation over summer months. Yet they are similar to values (f_m in Eq. 5.31) obtained by comparing cumulative melt to positive degree days. As discussed in the preceding section, f_m is typically 3 to $8\,\mathrm{mm\,day^{-1}\,°C^{-1}}$ for the Greenland Ice Sheet; the low value is typical for snow, the high value for ice. The data shown in Figure 5.7 gave a value of $5\,\mathrm{mm\,day^{-1}\,°C^{-1}}$ at a mid-latitude glacier, where the surface was ice but periodically covered by snow.

A rough theoretical value for the direct increase of ablation with warming can be obtained from the energy flux relations. Net energy should increase with temperature by at least the following three mechanisms:

1. Equation 5.27 suggests that the sensible heat flux should increase, for every degree of warming, by $0.0129 C^* P u$. For typical values, $C^* = 2 \times 10^{-3}$, windspeed of $5\,\mathrm{m\,s^{-1}}$, and elevation of 2000 m, the increase is $11\,\mathrm{W\,m^{-2}}$ for one degree. This flux would melt about 3 mm of ice in one day.

2. From Eq. 5.8, the increase of downward longwave radiation for a temperature change ΔT_a (small compared to T_a) should be approximately $4\epsilon_a \sigma T_a^3 \Delta T_a$. In terms of $E_L^{\downarrow}$, the total downward longwave before the change, it is $4E_L^{\downarrow}\Delta T_a / T_a$. Using values for a mid-latitude glacier (Table 5.3), this amounts to about $4\,\mathrm{W\,m^{-2}}$ for one degree of warming, enough to melt an additional 1 mm of ice per day.

3. Increased melt from the previous two factors hastens the exposure of ice as the winter snowpack disappears. Earlier exposure of ice, in turn, increases the shortwave absorption. The following calculation gives a rough idea of how important this is. For albedos of ice and snow of 0.3 and 0.6, respectively, and a daily mean downward shortwave flux of $250\,\mathrm{W\,m^{-2}}$, the ice surface would absorb about $75\,\mathrm{W\,m^{-2}}$ more than the snow surface (daily average). Mid-latitude ablation zones typically melt at 2 to 10 cm per day. The additional 4 mm per day

from sensible and longwave forcings corresponds to a 4% to 20% increase in daily melt. If it normally takes six weeks of melt for the winter snowpack to disappear, the increased melt implies two to nine extra days of ice exposure. In each of these days, the net shortwave flux is enhanced by about 75 W m^{-2}. Assume the entire melt season is 100 days. The increase of net shortwave absorption, averaged for the melt season, is thus 2 to 7 W m^{-2}. This corresponds to an additional 0.5 to 2 mm of ice per day, averaged over the melt season.

Thus, from rough theoretical considerations, the three mechanisms should increase melt by 4 to 6 mm of ice per day, given a warming of one degree. Empirical values for ice surfaces tend to be larger – about 8 mm day^{-1} °C^{-1} – probably because of additional factors that are difficult to estimate simply. Warming favors rain over snow, reducing surface albedos directly and through earlier exposure of ice. Warmer air in winter and spring results in faster warming of ice and snow and earlier onset of melting conditions.

Regardless, all of these values, theoretical and empirical, are consistent to within a factor of a few. They give a general indication of how much annual ablation should increase due to summer warming; with 100 days of melt per year, the increase is 0.4 to 0.8 m from one degree of warming. The number of days of melt will also increase with warming, however. Consider a simple description of the annual air temperature variation (Reeh 1991), such as

$$T_a = \overline{T}_a - A_T \cos(2\pi t) + G(0, \sigma) \tag{5.33}$$

where t measures time in years (zero in mid-winter), and $G(0, \sigma)$ is a random Gaussian fluctuation (mean of zero, standard deviation of σ) of daily temperature about the overall sinusoidal trend. Mean summer temperatures can increase with the mean annual temperature $\overline{T}_a$ or with the amplitude of the seasonal cycle A_T. Positive degree days can increase, in addition, with the variability of daily temperatures. The change in total melt dm_s from a change in positive degree days dD is

$$dm_s = \frac{\partial m_s}{\partial D} dD = f_m \left[\frac{\partial D}{\partial \overline{T}_a} d\overline{T}_a + \frac{\partial D}{\partial A_T} dA_T + \frac{\partial D}{\partial \sigma} d\sigma \right]. \tag{5.34}$$

Figure 5.9 shows how the positive degree days, and hence ablation, increase with mean annual temperature according to the annual cycle given by Eq. 5.33. The increase is nonlinear (over the whole range of temperatures), and the magnitude significant (considering melt-factor values) for mean annual temperatures greater than about −5 °C. This explains, succinctly, why the surface mass balance becomes strongly negative on a glacier flowing into a warm region, a fact shown clearly by the data in Figure 4.6b. Although those data also reflect differences in precipitation and other factors, they clearly show that, on average, annual melt in typical temperate-region ablation zones increases by 1 to 1.5 m per degree of warming. This observation is consistent with the simple degree-day model of Figure 5.9 for mean temperatures greater than −5 °C, assuming a surface of ice ($f_m = 8$ mm day^{-1} °C^{-1}). To see this, Table 5.6 gives the increase of annual melt per degree of warming for several environments, according to Figure 5.9. Note that,

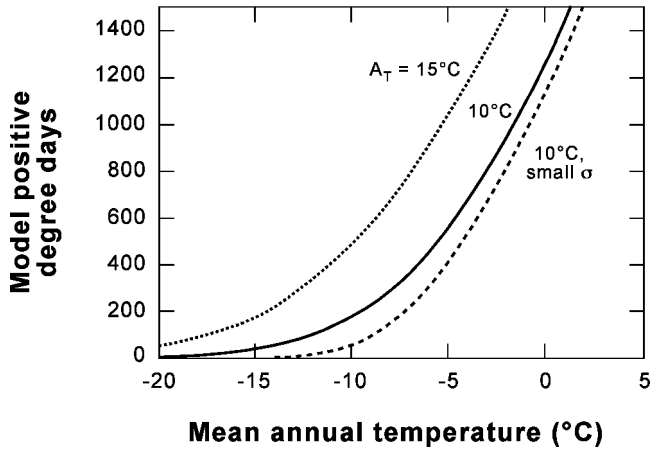

Figure 5.9: Increase of positive degree days with mean annual temperature, according to Eq. 5.33, for annual cycle amplitudes of 15 and 10 °C and $\sigma = 5$ °C. Variability was reduced to $\sigma = 2.5$ °C for the curve labelled "small σ." At temperatures greater than about −5 °C, the increase is approximately linear. Based on concepts developed by Reeh (1991).

Table 5.6: Theoretical sensitivity of melt to warming, for a surface of ice.

$\overline{T}_a$ (°C)	Melt increase (m °C^{-1})	
	$A_T = 10$ °C	$A_T = 15$ °C
−10	0.34	0.64
−5	0.86	1.1
0	1.4	

although the theoretical ablation increases nonlinearly over the whole range of temperatures, it can be well approximated by a linear function over intervals of 5 °C or so, the size of a large climate change.

An increase of ablation by 1 to 1.5 m yr^{-1} per degree of warming (and less at lower temperatures, as shown in the table) generally matches the values for the glacier-wide sensitivity of surface mass balance to temperature, the parameter C_T discussed in Section 4.2.6. In temperate and subpolar regions, that sensitivity largely manifests the increase of melt with temperature.

5.4.3.1 Total Ablation and Warming

Note that all the preceding discussion concerns the short-term effect of warming on surface ablation – specifically, the increase that could occur in a single year. The total increase of ablation due to warming can be much larger, for two reasons:

1. Warming sometimes enhances glacier flow. If sustained for years, enhanced flow can significantly reduce a glacier's surface altitude, causing additional warming and increased ablation.
2. Even without enhanced flow, a sustained increase of ablation lowers surface altitudes and so increases ablation further.
3. Warming can increase ice flow to termini in the ocean or deep lakes, significantly increasing calving.

These factors are discussed in Chapter 11.

5.4.4 Importance of the Frequency of Different Weather Conditions

The simple relations discussed in the previous section give a useful rough indication for how much the ablation increases when the climate warms. They are so generalized, however, that they obscure the diversity of processes governing the ablation – processes that vary greatly from place to place and over time. Moreover, when the climate changes, many factors change in addition to temperature. Most of the terms in the energy budget depend strongly on weather conditions. Even under similar conditions, their relative importance changes during the summer. To understand rigorously the causes of ablation, and its variations from year to year, the energy budget for the entire ablation season must be known. Thus, in principle, it is necessary to determine the relative frequency of different weather conditions, and the values of the energy budget terms associated with each at different times of the season.

Table 5.7 illustrates how the energy budget terms can vary in different weather situations at one location. These data, from Devon Island Ice Cap in Arctic Canada, are means over 7 to 12 days, at a location just above the equilibrium line (Holmgren 1971). Three common weather situations here are referred to as Types A, B, and C. Type A conditions involve cool and calm weather; little ablation occurs. Such conditions prevail when low pressure is centered east of Devon Island. In contrast, when cyclones track over Devon Island, winds are strong and warm

Table 5.7: Surface heat fluxes at Devon Ice Cap Station under different weather types. All fluxes are in W m^{-2}. Data from Holmgren (1971, Part F, p. 34).

Type	Sky	Wind	Surface	E_R	E_H	E_E	E_N
A	Clear	Light	Frozen	12	13	−5	20
A	Overcast	Light	Frozen	23	−4	−6	13
B	Overcast	Strong	Melting	45	46	10	101
C	Clear	Light	Melting	44	14	5	63
C	Clear	Light	Frozen	4	16	−6	14

Table 5.8: Energy budgets in Antarctica ($W\,m^{-2}$).

Site	Elevation	Season	E_R	E_H	E_E	Reference
Vostok	3400 m	Summer	32	−25	−2	Artemyev (1973)
		Winter	−17	15	0	
Mizuho	2230 m	Summer	20	−7	−8	Ohata et al. (1985)
		Winter	−38	37	0	
Maudheim	37 m	Summer	9	6	†	Liljequist (1957)
		Winter	−22	13	†	

† Not measured.

moist air flows over the ice cap (Type B conditions). The surface receives long-wave radiation from clouds and an increased flux of sensible heat; ablation is substantial. Type C conditions are anticyclonic, with clear skies that promote downward solar radiation. The effect of Type C conditions depends on whether the surface is melting or not. When it is, low albedos increase the absorption of solar radiation. Such conditions produce intense ablation at lower altitudes where bare ice is exposed (Alt 1978). Overall, the ice cap has a positive annual mass balance when Type A cyclonic conditions dominate the summer weather pattern. In contrast, a season in which Type C anticyclonic conditions predominate can produce enough ablation to eliminate the positive balance of five seasons of Type A.

5.4.5 Energy Budget Regimes

The example from Devon Island discussed in the previous section illustrates the energy budget near the equilibrium line on an Arctic ice cap. We now briefly discuss other environments.

5.4.5.1 Antarctica and the Coldest Sectors of Greenland

Where the climate is so cold that melt rarely occurs, net energy instead warms or cools the surface and underlying layers. Ablation occurs by sublimation, which is favored by dry air, a warm surface, and strong winds (Section 5.3.6.8). Table 5.8 shows energy budget data for three sites in East Antarctica. Vostok is in the interior, Mizuho about 375 km from the coast, and Maudheim on an ice shelf. Summer values are means for December and January, winter values for June and July.

In winter, because there is no solar radiation, the term E_R equals the net longwave radiation. At the two inland stations sensible heat fluxes almost balance the longwave radiation. Winter-time sensible heat flux is particularly high at Mizuho as a result of turbulence created by strong katabatic winds; these also produce significant evaporation in summer. Because there is little melting at Maudheim and none at the other sites, the net positive fluxes are used solely to warm the surface and the layers beneath.

Table 5.9 compares the summer energy budget, now in greater detail, for snow and blue ice sites (Bintanja 2000). Values are averages from a 37-day period. Mean elevation of snow sites was about 1500 m and for ice sites about 1200 m.

During summer, daily totals of $E_S^{\downarrow}$ are comparable to mid-latitude values because of perpetual sunlight. The surface sublimates most rapidly at this time, because its relatively high temperature tends to increase the vapor pressure gradient (the term $e_s - e$ in Eq. 5.28). Sublimation is more rapid on bare ice than on snow. Such "blue ice zones" cover about 1% of Antarctica (Winther et al. 2001). Compared to snow-covered sites, the blue ice sites absorb more solar radiation because of their lower albedos. At the blue ice sites, the summertime sublimation rate was about 0.3 m yr^{-1}, about three times greater than at the snow sites.

5.4.5.2 Mid-latitudes

On mid-latitude glaciers in summer, high values of net radiation and sensible heat flux drive rapid melt. We have already discussed the time-varying energy budget at one such site in the Canadian Rockies (Figures 5.4, 5.6, and 5.7); we now introduce another site, where we can compare energy budgets for the ablation and accumulation zones. Exceptionally thorough energy budget studies have been conducted on Pasterze Gletscher, Austria's largest glacier (latitude 47 °N). Altitudes range from 2200 to 3400 m. Table 5.10 summarizes data from this site, acquired by a network of five automatic weather stations for a 46-day period in mid-summer of 1994 (Greuell and Smeets 2001). Shown separately are averages for accumulation zone sites and ablation zone sites. At the former, snow persisted throughout the measurement period. At the latter, ice was exposed by the end of the period.

Table 5.9: Summer energy budget (W m^{-2}) for snow and blue ice areas in Dronning Maud Land, Antarctica (Bintanja 2000). Values are averages for N sites in each row.

Sites	α_s	$E_S^{\downarrow}$	E_S^{Net}	$E_L^{\downarrow}$	$E_L^{\uparrow}$	E_L^{Net}	E_R	E_H	E_E	E_G	N
Snow	0.82	334	63	185	−254	−69	−6	16	−9	−1	4
Blue ice	0.64	356	121	192	−279	−87	34	2	−26	−11	3

Table 5.10: Mean energy budget terms from a 46-day melt-season study on Pasterze Gletscher, Austria (data aggregated from Greuell and Smeets (2001) by S.J. Marshall). All fluxes are in W m^{-2}. Average altitudes of ablation and accumulation zone sites were 2312 and 3085 meters, respectively.

Sites	α_s	$E_S^{\downarrow}$	E_S^{Net}	$E_L^{\downarrow}$	$E_L^{\uparrow}$	E_L^{Net}	E_R	E_H	E_E	E_N	T_a (°C)	z_0 (mm)
Ablation	0.25	269	201	298	−315	−17	184	55	10	249	6.8	3.2
Accum.	0.60	297	120	278	−314	−36	85	22	3	109	3.4	1.7

Peak daytime values of downward solar radiation in the mid-latitudes are as high as about 1000 W m^{-2}, higher than possible in polar regions. The daily averages of $E_S^{\downarrow}$ are not very different from mid-summer in Antarctica, however. The high net radiation ($E_{\mathbf{R}}$) at mid-latitude sites is instead, as the Pasterze Gletscher example shows, due to lower albedo and to larger downward longwave fluxes. Because longwave emissions from the atmosphere depend on both temperature and moisture, the warmer and moister atmosphere of the mid-latitudes is a strong energy source compared to the polar atmosphere. Losses of longwave from the surface, on the other hand, are constrained by the melting temperature. In addition, because of the warm atmosphere Pasterze Gletscher receives a much larger sensible heat transfer than do the Antarctic sites, although comparable to fluxes on Arctic ice caps in warm weather (Table 5.7).

On Pasterze Gletscher, net radiation decreases with increasing altitude, because of albedo; snow perpetually covers the higher parts of the glacier. Sensible and latent heat fluxes also decrease with altitude as a result of cooler air and reduced vapor pressure. The mean net energy flux in the ablation area (249 W m^{-2}) corresponds to a melt rate of 0.07 m day^{-1}, or about 2 m in one month.

5.4.5.3 Low-Latitude Glaciers

All low-latitude glaciers occur at high altitudes.

The energy budget of glaciers in the low-latitude subtropics is similar to that of mid-latitude glaciers, but with even greater magnitudes of fluxes in some regions. Consider one example from the Karakoram in Pakistan, a high-elevation region with a dry climate. At 4300 m altitude on Chogo-Lungma Glacier, Untersteiner (1975) estimated daily mean net radiation of $E_{\mathbf{R}} \approx 190$ W m^{-2} and a sensible heat flux of about $E_H \approx 120$ W m^{-2}. Some of these high-altitude glaciers also have very large energy losses due to evaporation, a consquence of dry air and strong winds; Bai and Yu (1985) reported latent heat losses as large as 58 W m^{-2} on firn at 4750 m on Mount Muztagata in China. This is a particularly important process affecting ablation of glaciers in the tropics, discussed next.

Most tropical glaciers are in the Andes, but some exist in East Africa and New Guinea. The climate here is quite different from that of the mid-latitudes; the implications for glacier regimes have been elaborated by Kaser (2001) and Kaser and Osmaston (2002). Temperature varies little with season but precipitation and atmospheric moisture do. Seasonal migration of the intertropical convergence zone produces one wet season per year in the outer tropics but two in the inner tropics (the "inner" zone being centered on the equator). Air temperatures above melting point are rare on glaciers of the highest Andean summits and Mt. Kilimanjaro, Africa (Thompson et al. 1984, 1995; Kaser et al. 2004; Mölg et al. 2008a).

Snowfall occurs mostly in the wet seasons but, in the outer tropics, the wet season is also the primary ablation season (Wagnon et al. 1999a, 1999b, 2003). Temperatures are a little warmer in this season, but the key process appears to be reduced consumption of energy by sublimation. Sublimation occurs most rapidly in the dry season; Wagnon et al. (1999b) reported average sublimation rates of 1.1 mm day^{-1} in the dry season in the Andes, but less than

0.3 mm day^{-1} in the wet season. Sublimation has a large energy cost in the dry season; most of the energy supplied to the surface by net radiation and sensible heat is consumed by sublimation, leaving little energy for melting. The latent heat of sublimation is 8.5 times greater than that for melt. Thus sublimation acts as a strong energy sink but an ineffective ablation mechanism. For example, an energy surplus of 50 W m^{-2} will, over one month, ablate 35 cm of ice if used for melt, but only 4.1 cm of ice if used for sublimation. Furthermore, sensible heat flux tends to be small at these sites because of persistently cold air temperatures related to the very high altitudes. The same conditions apply to the glaciers high on Kilimanjaro in the inner tropics (Mölg and Hardy 2004; Mölg et al. 2008a). On Kilimanjaro's flanks, atmospheric moisture increases down-glacier, reducing the sublimation energy sink; ablation thus increases (Mölg et al. 2008b).

On tropical glaciers with comparatively low altitudes, however, changes of atmospheric moisture act in an entirely different way. An increase of atmospheric moisture probably reduces ablation; increased cloudiness reduces the downward solar radiation, and more snowfall causes higher albedos and reduced shortwave absorption at the surface. Thus, if the climate becomes increasingly arid, not only would accumulation decrease but ablation would increase. This is one explanation for the twentieth-century retreat of glaciers in East Africa (Kruss and Hastenrath 1987; Kaser et al. 2004). On the much shorter timescale of diurnal cycles, convective cloud formation in the afternoon reduces ablation and increases precipitation on western slopes (Hastenrath 1991; Mölg et al. 2003a). This helps to explain the more extensive ice cover on western slopes in the tropics.

Table 5.11 summarizes the energy budget on Zongo Glacier in the Cordillera Real, Bolivia, at latitude 16.25 °S (Wagnon et al. 1999b). These measurements are from a site at 5150 m altitude, near the mean ELA. The net radiation and sensible heat inputs are both small compared with those on mid-latitude and subtropical glaciers in summer. The net longwave flux is particularly negative, due to the cold, dry, and low-density air at high altitude. Most notable is the large fraction of ablation energy consumed by sublimation (the variable f_E); it is about 90% in the dry season. Field measurements of ablation and runoff at this site agree well with estimates based on the energy budget.

Table 5.11: Energy balance and meteorological data from Zongo Glacier, Bolivia (Wagnon et al. 1999a). Data are for the hydrological year September 1996 to August 1997. Wet and dry seasons are November–February and May–August, respectively. All fluxes are in W m^{-2}.

Period	α_s^1	$E_S^{\downarrow}$	E_S^{Net}	E_L^{Net}	E_R	E_H	E_E	T_a (°C)	q (g/kg)	m_s (mm)	Subl. (mm)	f_E
Wet season	0.66	196	67	–54	13	4	–7	–0.3	5.8	327	27	0.41
Dry season	0.52	220	106	–95	11	9	–31	–3.8	4.4	107	117	0.90

[1] Based on the mean measured daily minimum albedo.

On tropical glaciers, many of the meteorological variables change greatly through diurnal cycles (Mölg et al. 2008a). But variations from day to day and over the seasons are much reduced compared to those on extra-tropical glaciers, and ablation is not confined to a summer season. Furthermore, as the preceding discussion should make clear, ablation at high-altitude sites only indirectly relates to temperatures, if at all. For these reasons, the positive degree-day approach to modelling ablation should not work; instead, the full energy budget needs to be calculated, at a high enough time resolution to resolve different parts of the daily cycle.

Further Reading

The book by Oerlemans (2001) is the major recent analysis of how the surface energy budget relates to glacier mass balance. It also discusses the relation between regional climate and local climate of the glacier surface, a topic not covered here. Hartmann (1994) gives a good introduction to global climatology; Wallace and Hobbs (2006) provide a readable introduction to atmospheric radiation and dynamics. The books by Stull (1988) and Garratt (1992) discuss boundary layer meteorology, a helpful resource for learning about energy budgets.